Applications of knot theory to the detection of heteroclinic connections between quasi-periodic orbits

Danny Owen, Nicola Baresi

Surrey Space Centre, University of Surrey, Guildford, UK

ABSTRACT

Heteroclinic connections represent unique opportunities for spacecraft to transfer between isoenergetic libration point orbits for zero deterministic ΔV expenditure. However, methods of detecting them can be limited, typically relying on human-in-the-loop or computationally intensive processes. In this paper we present a rapid and fully systematic method of detecting heteroclinic connections between quasi-periodic invariant tori by exploiting topological invariants found in knot theory. The approach is applied to the Earth–Moon, Sun–Earth, and Jupiter–Ganymede circular restricted three-body problems to demonstrate the robustness of this method in detecting heteroclinic connections between various quasi-periodic orbit families in restricted astrodynamical problems.

KEYWORDS

CR3BP
quasi-periodic torus
heteroclinic connection
knot theory

Research Article

Received: 18 September 2023
Accepted: 16 January 2024

1 Introduction

The past few decades have on many occasions demonstrated the importance of multi-body dynamics in the design of space mission trajectories, allowing us to produce orbits and transfers that would be impossible in lower-fidelity models such as patched conics. This is incredibly important when designing trajectories in the cislunar region, where many upcoming missions aim to operate. One such class of trajectories unique to multi-body dynamics are heteroclinic connections, which will be the focus of this paper.

The Genesis mission famously made use of a heteroclinic connection between Sun–Earth L1 and L2 libration orbits [19]; this transfer trajectory allowed the spacecraft to travel between distant regions of space with zero deterministic ΔV cost. As such, these methods offer a unique opportunity to extend the life of missions when an operational spacecraft has minimal remaining fuel for large orbit changes; THEMIS-ARTEMIS was the extension of the THEMIS mission, during which two of the spacecraft were placed into Lissajous orbits and performed heteroclinic connections between L1 and L2 libration point orbits at the Moon [4, 8]. Now attention has returned to the Moon with the advent of NASA's Artemis program, the successor to the Apollo program, which aims to land humans on the Moon before the end of the decade [29]. In addition, the Lunar Gateway promises to be an international collaboration to construct a science and habitation module in lunar orbit. For these reasons, new mission design techniques for fuel-minimal trajectories in the vicinity of the Moon are of great interest. Heteroclinic connections have been proven to provide such opportunities.

Heteroclinic connections exist at the intersections of a stable and an unstable manifold, each manifold belonging to a different object such as an equilibrium point, or periodic or quasi-periodic orbit. As the unstable manifold naturally departs from one orbit and the stable manifold naturally arrives at another, this allows a spacecraft to traverse between them without the need for any fuel expenditure. While heteroclinic connections between periodic orbits exist, they can be shown to be rare due to the low dimensionality of the intersecting manifolds.

The dimension of intersection of two manifolds is found by subtracting the sum of the co-dimensions of the two manifolds from the dimension of the phase space; the co-dimension of the manifolds themselves are found by subtracting the dimension of a manifold from the

✉ danny.owen@surrey.ac.uk

dimension of the phase space. Performing an analysis of the dimension of intersection of invariant manifolds emanating from both periodic and quasi-periodic orbits (Tables 1 and 2), we find quasi-periodic orbit manifolds to have a higher dimension of intersection. This suggests heteroclinic connections are more common between quasi-periodic orbits than periodic orbits, which is supported by existing research [18]. For this reason quasi-periodic orbits will be the focus of this work, as connections between them are more prevalent.

While heteroclinic connections could prove incredibly useful for future lunar missions and far beyond, producing them is often difficult, time-consuming, or computationally intensive with current methods, both for periodic and quasi-periodic orbits.

Gómez *et al.* and Arona and Masdemont's approach to detecting heteroclinic connections was to expand the Hamiltonian of Hill's problem near libration points in normal forms. However, this process fails to elegantly tackle the dimension problem, instead relying heavily on numerical procedures to search the design space for heteroclinic connections [5, 13, 14]. In addition, this method is limited in robustness as it fails to approximate accurately the dynamics far from the libration points. Barcelona, Haro, and Mondelo used parameterisation methods to compute Taylor expansions of stable and unstable manifolds of periodic orbits, generating large "meshes", making the structure of the manifolds explicit [6]. However, when looking for connections between these orbits, the Euclidean distance between points in two sets of manifold states are calculated and minima are extracted to find initial guess trajectories for further correction. This is method of finding initial guesses for connection has been common in several other studies of the problem regardless of how the compared manifold sets are generated; specifically, the past work of Masdemont, Delshams, and Roldán [12, 23]. This approach can be successful but does not guarantee a thorough search of all possible connections.

Instead, a common approach is to choose to represent one or more of the dimensions in novel ways. Anderson and Lo have done much work on producing heteroclinic connections in the Jupiter–Europa system [2, 3] using Poincaré maps, however much of this work is completed in the planar problem, reducing the dimensions by 2 but limiting overall mission design opportunities. Kumar and de la Llave take a similar approach, producing heteroclinic connections in planar models of the Jovian system using Poincaré maps [21]. Additionally, these works present connections between periodic orbits, not quasi-periodic orbits. Haapala and Howell tackled the problem by selecting two of the dimensions to be represented as vectors originating from data points in the other two dimensions [16], as well as extracting and plotting the perilune of manifold trajectories [15]. These are also implemented to find connections between periodic orbits, not quasi-periodic orbits; however, McCarthy and Howell adapted the velocity vector representation method from Ref. [16] to the manifolds of quasi-periodic orbits [24]. Bonasera and Bosanac made use of an algorithm known as Uniform Manifold Approximation and Projection (UMAP) to construct a lower-dimensional representation of the intersection states, projecting high dimensional data into lower dimension space [7]. These dimension reduction techniques allowed them to find connections between quasi-periodic orbits, but restrict the user to a human-in-the-loop regime.

Another approach to detecting heteroclinic connections between periodic orbits was taken by De Smet and Scheeres, who implemented machine learning algorithms

Table 1 Dimensional analysis for periodic orbit manifolds

	Stable manifold	Unstable manifold		
Dimension	2	2	5	Dimension, phase space
Co-dimension	3	3	6	Co-dimension, intersection
			−1	Dimension, intersection

Table 2 Dimensional analysis for quasi-periodic orbit manifolds

	Stable manifold	Unstable manifold		
Dimension	3	3	5	Dimension, phase space
Co-dimension	2	2	4	Co-dimension, intersection
			1	Dimension, intersection

to circumvent the restriction of a human-in-the-loop regime [11]. However, while excellent at handling high-dimensional data, machine learning algorithms offer little insight into the dynamical properties of a solution. Care must also be taken in tuning the parameters of a machine learning algorithm, as well as discarding false positives. In addition, large swathes of training data are required to train such an algorithm to a useful level of accuracy.

Olikara made use of an "indirect" computation [25], expanding the work of Calleja [9] from periodic to quasi-periodic connections, wherein a binary search algorithm and differential corrector are used to extend the time a departing manifold spends in the region of the arrival torus. However, the numerical procedures have been shown to fail in certain situations, such as if the trajectory being corrected arrives tangential to the stopping plane which determines the region of the arrival torus.

Many of these methods will inevitably, due to numerical errors or interpolation, provide trajectories that are close to, but not exactly, heteroclinic connections, which we will call "initial guess trajectories". These initial guess trajectories provide excellent approximate solutions for refinement by differential correction methods. This has been demonstrated notably by Henry and Scheeres [17]. In their work, a system of boundary constraints are formed for which the variables are defined by the location of manifold trajectory initialisation on the surfaces of the departure and arrival tori, parameterised by the four torus angles, as well as the two propagation times of the manifold trajectories. Assuring these trajectories have equal states after propagation ensures a heteroclinic connection. Henry and Scheeres approach the problem of producing an initial guess for the differential correction by first finding intersections between the stable and unstable manifolds in position space. The norm of the difference in velocity at each point in that intersection region is then calculated. Points with a velocity difference below some tolerance at taken as approximate solution. The work demonstrates the benefit of a combined detection and correction methodology, and a similar approach to differential correction will be taken later in this work. However, this process still relies on selecting initial guesses based on near-zero differences in velocity in those intersection regions, which could lead to false minima.

The method presented in this work aims to circumvent all of the above issues by exploiting topological properties of the invariant manifolds of two orbits to quickly generate initial guess trajectories for later differential correction. This allows for robust detection of heteroclinic connections between quasi-periodic orbits.

2 Background

2.1 Linking number

The linking number is a topological invariant used in knot theory to describe how many times two closed curves in 3-dimensional space wrap around one another [27, 28]. As a topological property, the linking number is equal for any two pairs of closed curves for which one pair can be made into the other pair via continuous deformation, assuming the curves do not cross during this process. Therefore, the *only* way the linking number can change is if the curves pass through each other. A linking number of 0 means that the curves can be continuously deformed to become a pair of entirely separate circles without the need to pass through each another. A pair of circles linked like a section of chain would have a linking number of 1 or -1, depending on the orientation of the curves.

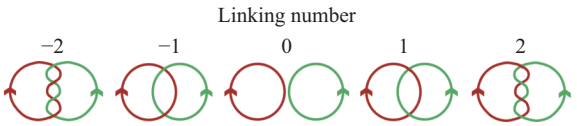

Fig. 1 Simple curves which are isomorphic to all curves with linking numbers between -2 and 2.

Linking number equivalents exist for dimensions beyond 1-dimensional curves in 3-dimensional space [28]. In general, a linking number can be calculated to describe the relationship of any two closed manifolds of dimensions m and n, so long as the dimension of the space they are embedded within d satisfies the equation $d = m + n + 1$. In this work, we will be considering 1-dimensional closed manifolds in 3-dimensional space only. The linking number is calculated by constructing a surface bounded by one of the curves and tracking the number and direction of intersections between this surface and the other curve, described in further detail in Section 3.1.

2.2 Circular restricted three-body problem

The circular restricted three-body problem (CR3BP) is a simplified model of the dynamics of three bodies, where one of the bodies is a satellite and taken to be much smaller than the other two, which in this work

this will often be the Earth and Moon. We only consider the influence of the primary and the secondary on a spacecraft, denoted P_1, P_2, and P_3 respectively. This model is a good approximation of the dynamics in cislunar space and allows for useful exploitation of dynamical systems theory in mission design. Some assumptions are made; the orbit of the Moon about the Earth is assumed to be circular, and the mass of the spacecraft is assumed to be zero [20].

We normalise the problem by selecting units of distance and time such that both the distance between the Earth and Moon and the reciprocal of the Moon's angular velocity are both 1. We additionally define a mass ratio parameter μ, where

$$\mu = \frac{m}{M+m} \tag{1}$$

Here, m and M are the mass of the Moon and Earth respectively. A rotating reference frame is selected with an origin at the barycenter of the Earth and Moon. The rotation rate of the frame is equal to the angular velocity of the Moon's orbit; this means that the Earth and Moon appear stationary positioned on the x-axis, located at coordinates $[-\mu, 0, 0]$ and $[1-\mu, 0, 0]$ respectively. The y-axis is parallel to the direction of the Moon's velocity, and the z-axis is perpendicular to the x–y plane.

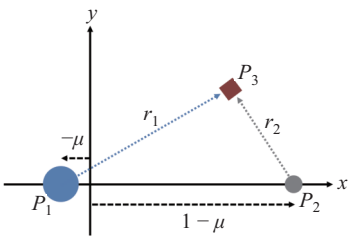

Fig. 2 Circular restricted three-body problem.

The equations of motion of the system are given by [10]:

$$\ddot{x} - 2\dot{y} = x - \frac{1-\mu}{r_1^3}(x+\mu) - \frac{\mu}{r_2^3}(x+\mu-1) \tag{2}$$

$$\ddot{y} + 2\dot{x} = y - \frac{1-\mu}{r_1^3}y - \frac{\mu}{r_2^3}y \tag{3}$$

$$\ddot{z} = -\frac{1-\mu}{r_1^3}z - \frac{\mu}{r_2^3}z \tag{4}$$

where the spacecraft state $\boldsymbol{X}$ is described by $[x, y, z, \dot{x}, \dot{y}, \dot{z}]$ and r_1 and r_2 are the positions of the spacecraft relative to the primary and secondary respectively.

The CR3BP admits a single integral of motion C, known as the Jacobi integral [20]. A constant such as this proves useful in mission design by narrowing the design space, allowing us to define in advance the "energy" of a state and thus reduces the number of variables that must be known at a later state after propagation.

$$C = \Omega - \frac{\dot{x}^2 + \dot{y}^2 + \dot{z}^2}{2} \tag{5}$$

where

$$\Omega = \frac{1}{2}(x^2+y^2) + \frac{1-\mu}{r_1} + \frac{\mu}{r_2} \tag{6}$$

The Jacobi integral of a trajectory determines which regions of space the spacecraft can access; additionally, in the CR3BP, heteroclinic connections can *only* exist between orbits that are of the same Jacobi integral, known as isoenergetic orbits.

2.3 Quasi-periodic tori

The focus of this work is on quasi-periodic orbits, specifically of dimension 2. As 2-dimensional objects they can be parameterised by two torus angles, θ_0 and θ_1, or longitudinal and latitudinal respectively. For any given torus in the CR3BP, the function that maps its torus angles $\boldsymbol{\theta} = [\theta_0, \theta_1]$ to state space coordinates $\boldsymbol{X} = [x, y, z, \dot{x}, \dot{y}, \dot{z}]$ is achieved via the torus function $\boldsymbol{U}(\boldsymbol{\theta}) = \boldsymbol{X}$ [25]. For heteroclinic connections to exist between orbits they must be isoenergetic; quasi-periodic tori exist in 2-parameter families with variable energy and ratio of fundamental frequencies. Setting the Jacobi integral of the tori as constant, they then exist in 1-parameter families defined by their unique ratio of fundamental frequencies. For this work numerical methods for generating quasi-periodic tori developed by Gómez, Mondelo, Olikara, and Scheeres (GMOS) [26] were implemented. This method has the benefit of providing stability information via the Floquet matrix, generated torus as a byproduct of the scheme, which can be later used to produce the hyperbolic manifolds of the torus.

The hyperbolic manifolds of a torus are of one dimension higher than the torus itself. In the case of 2-dimensional tori, the manifolds are 3-dimensional objects. These manifolds can be found numerically by considering the Floquet matrix of the torus and extracting the eigenvectors associated with the stable and unstable eigenvalues at a given location on the surface. These stable and unstable eigenvectors $\delta\boldsymbol{U}_\mathrm{s}(\boldsymbol{\theta})$ and $\delta\boldsymbol{U}_\mathrm{u}(\boldsymbol{\theta})$ are used to perturb states along the torus by some arbitrary scaling factor, ϵ, set in this work to 1×10^{-6}. This method

allows us to generate two new tori associated with the initial torus, which are defined by all points on the initial torus surface after being perturbed onto the stable or unstable manifold. The function that maps the torus angles of the original torus to equivalent state space coordinates that exist on the surface of these "perturbed objects" will be referred to as the manifold functions $\tilde{\boldsymbol{U}}_{\mathrm{s}}(\boldsymbol{\theta}) = \boldsymbol{U}(\boldsymbol{\theta}) + \epsilon\delta\boldsymbol{U}_{\mathrm{s}}(\boldsymbol{\theta})$ and $\tilde{\boldsymbol{U}}_{\mathrm{u}}(\boldsymbol{\theta}) = \boldsymbol{U}(\boldsymbol{\theta}) + \epsilon\delta\boldsymbol{U}_{\mathrm{u}}(\boldsymbol{\theta})$, where the subscripts s and u refer to the stable and unstable manifolds respectively.

Torus maps provide a unique way to understand the manifolds of quasi-periodic orbits. A torus map is a method of mapping the values of a continuous function to the surface of a torus. Positions on the torus map can be easily parameterised by the two torus angles, θ_0 and θ_1. For example, we can choose to map one of the state variables of the stable manifold after initialisation from the torus surface; that is, after it is perturbed onto the manifold and propagated numerically. Figure 3 is an example of such a map for the variable z, mapped to the surface of a quasi-halo orbit perturbed onto the stable manifold.

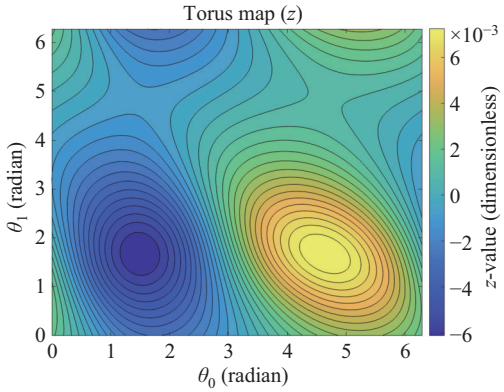

Fig. 3 Example torus map of z-values of a perturbed quasi-halo orbit at the Earth–Moon L2 point.

As this mapping is continuous, we can take level curves of the torus map. These curves represent all points on the map for which the height is equal to some selected value. For example, selecting $z = 0$ as the level curve, we can interpolate all values of θ_0 and θ_1 for which the height of the map is zero. We can then interpolate the height of the torus maps associated with x and y for those same values of θ_0 and θ_1, and determine the position states at which the torus intersects the $z = 0$ plane, as seen in Fig. 4; the red curves in both plots represent the level curves and the interpolated position states found using

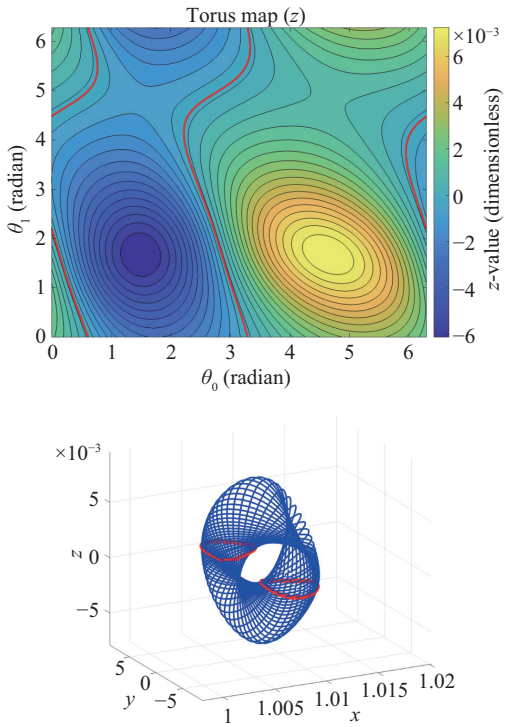

Fig. 4 Level curve of $z = 0$ extracted from the torus map in Fig. 3 used to interpolate position states.

said level curves. Interpolation of state variables along level curves in this way will be necessary later in this work when describing the methodology of our approach.

2.4 Manifold generation

The GMOS method of generating quasi-periodic tori provides a set of N 6×1 state vectors that lie on an invariant circle of the torus, each with equal longitude and with equally spaced latitude angles. We then produce M additional invariant circle sets at equally spaced longitude angles. Each of these invariant circles has an associated Floquet matrix which is extracted in the generation process and can be used to find $\delta\boldsymbol{U}_{\mathrm{s}}(\boldsymbol{\theta})$ and $\delta\boldsymbol{U}_{\mathrm{u}}(\boldsymbol{\theta})$ for points in the set. The eigenvectors extracted are 6 $N \times 1$ vectors, which are appropriately scaled and applied to $\boldsymbol{U}(\boldsymbol{\theta})$ to produce states which can be propagated to find trajectories that exist within the manifold of the torus. Performing this for each invariant circle, we have two sets of $N \times M$ states for trajectories initialised onto the stable manifold and unstable manifolds. Given these sets, it is easy to initialise manifold trajectories from any point on the tori surfaces by constructing torus maps using the state variables and interpolating the states for any value of the torus angles.

When propagating these resulting states, the stable manifold is propagated in backward time and the unstable manifold is propagated in forward time. They are propagated until they intersect the surface of section $x = 1 - \mu$, the x position of the Moon. The resulting sets of all trajectories in the stable and unstable manifolds are referred to as W_s and W_u.

2.5 Regularisation

Heteroclinic connections may often pass within the vicinity of a singularity, as is the case for connections between L1 and L2 libration orbits in the Earth–Moon system as the centre of the Moon is a singularity in the CR3BP. This can negatively impact the accuracy and computation time of common numerical methods when propagating trajectories in the lunar vicinity. In addition, this singularity can negatively affect the torus maps which map invariant manifold states at the surface of section to the point on the torus surface where the manifold trajectory was initialised; velocity variables can reach very high magnitudes when the manifolds pass very close to the Moon, drastically skewing the height of the torus maps in certain regions. These issues can be avoided by the use of regularised equations of motion, which introduce a fictitious time and removes one of the two singularities in the system [10]; in this work, we select the singularity at the Moon to be removed.

We define (q_1, q_2, q_3) as the physical space and (Q_1, Q_2, Q_3) as the parametric space. Note that as we are removing the singularity via the introduction of fictitious time and position is not related to time in the same way as velocity or acceleration, the physical variables (q_1, q_2, q_3) are equal to the equivalent standard coordinates (x, y, z), but $(\dot{q}_1, \dot{q}_2, \dot{q}_3)$ will vary from $(\dot{x}, \dot{y}, \dot{z})$. We will use the Kustaanheimo–Stiefel transformation [22] to construct our physical variables and equations of motion in regularised form.

In order to regularise the system around the Moon, we must define a matrix $A(Q)$ such that

$$\begin{bmatrix} q_1 \\ q_2 \\ q_3 \\ q_4 \end{bmatrix} = A(Q) \begin{bmatrix} Q_1 \\ Q_2 \\ Q_3 \\ Q_4 \end{bmatrix} + \begin{bmatrix} 1-\mu \\ 0 \\ 0 \\ 0 \end{bmatrix} \tag{7}$$

The elements of $A(Q)$ must be linear homogeneous functions of Q, and $A(Q)$ must be orthogonal. Hurwitz showed such a matrix for this application is only possible for spatial dimensions 1, 2, 4, and 8 [10, 30]. Therefore we must expand the parametric space to 4 dimensions, defining $A(Q)$ to be

$$A(Q) = \begin{bmatrix} Q_1 & -Q_2 & -Q_3 & Q_4 \\ Q_2 & Q_1 & -Q_4 & -Q_3 \\ Q_3 & Q_4 & Q_1 & Q_2 \\ Q_4 & -Q_3 & Q_2 & -Q_1 \end{bmatrix} \tag{8}$$

As our physical system is 3-dimensional, we can set Q_4 to zero. From this we find

$$Q_1 = \sqrt{\frac{q_1 + r_2 + \mu - 1}{2}} \tag{9}$$

$$Q_2 = \frac{q_2}{2Q_1} \tag{10}$$

$$Q_3 = \frac{q_3}{2Q_1} \tag{11}$$

As the position states in regularised and non-regularised coordinates are equal, r_2 here is the same as described in Section 2.2.

It is easily shown that the differential with respect to time $A(Q)' = A(Q')$ [10]. Therefore, we find the first and second derivatives of q to be

$$q' = 2A(Q)Q' \tag{12}$$

$$q'' = 2A(Q)Q'' + 2A(Q')Q' \tag{13}$$

We introduce a fictitious time s, defined using the scaling factor D.

$$\mathrm{d}t = D\mathrm{d}s \tag{14}$$

$$D = 4r_2 = 4(Q_1^2 + Q_2^2 + Q_3^2 + Q_4^2) \tag{15}$$

From these equations we can calculate the equations of motion of the CR3BP in this fictitious time to be

$$Dq_1'' - D'q_1' - 2D^2q_2' = D^3\Omega_{q1} \tag{16}$$

$$Dq_2'' - D'q_2' + 2D^2q_1' = D^3\Omega_{q2} \tag{17}$$

$$Dq_3'' = D^3\Omega_{q3} \tag{18}$$

By converting our physical state variables to the parametric state variables we can use ordinary differential equation solvers along with the above equations to numerically integrate the parametric state before converting the integrated values back to physical state variables where required. Figure 5 shows a numerically integrated L2 southern near-rectilinear halo orbit in the Earth–Moon system, produced via standard equations of motion and via regularised equations of motion. Note that the regularised propagation produces a lower density of integrated states. Computation time is improved with the regularised state formulation since less integration steps are required to produce the same trajectory.

The removal of the singularity is easily shown to

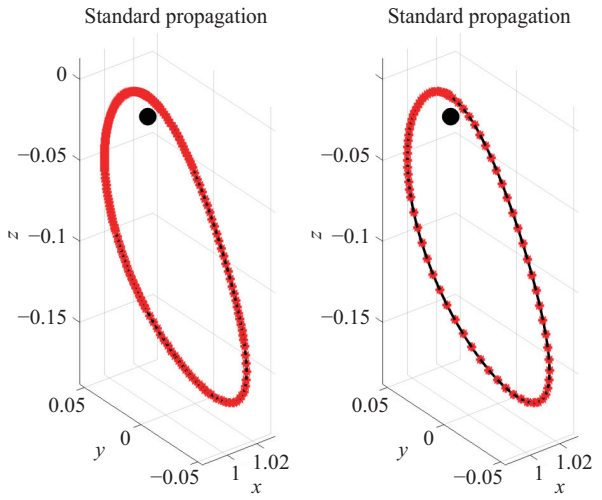

Fig. 5 Earth–Moon L2 NRHO propagated using standard and regularised equations of motion

improve the representation of the torus map after using the regularized coordinates instead of the non-dimensional rotating coordinates defined in Section 2.2. Propagating the invariant manifolds of a quasi-periodic torus until they intersect the surface of section defined by $x = 1-\mu$, we can then map the manifold states at the surface of section to the position of initialisation on the torus surface via a torus map. The height of the maps in Fig. 6 represent $\dot{y}$ and q_2' at the surface of section respectively. The torus map of $\dot{y}$ variables contains clear singularities. This makes interpolation of level curves on the map challenging and ultimately inaccurate. However, mapping instead the regularised q_2' variables, we find the torus map much easier to interpret and the results of interpolation from these maps behaves more consistently.

The surface of section $x = 1-\mu$ was selected as heteroclinic connections between libration orbits in the vicinity of L1 and L2 are explored in this paper. However, the choice of surface of section is arbitrary and dependent on the mission design engineer's needs.

While technically the torus maps used throughout the paper therefore use values of $\boldsymbol{q}$ to define the map height, we will be using x, y, z, $\dot{x}$, $\dot{y}$, and $\dot{z}$ to refer to q_1, q_2, q_3, $\dot{q}_1$, $\dot{q}_2$, and $\dot{q}_3$ for the sake of ease of understanding when using torus maps.

2.6 Heteroclinic connections

The stable manifold describes all the trajectories that will approach an invariant object as time t tends towards $+\infty$, while the unstable manifold describes the trajectories that will approach an invariant object as t tends towards $-\infty$.

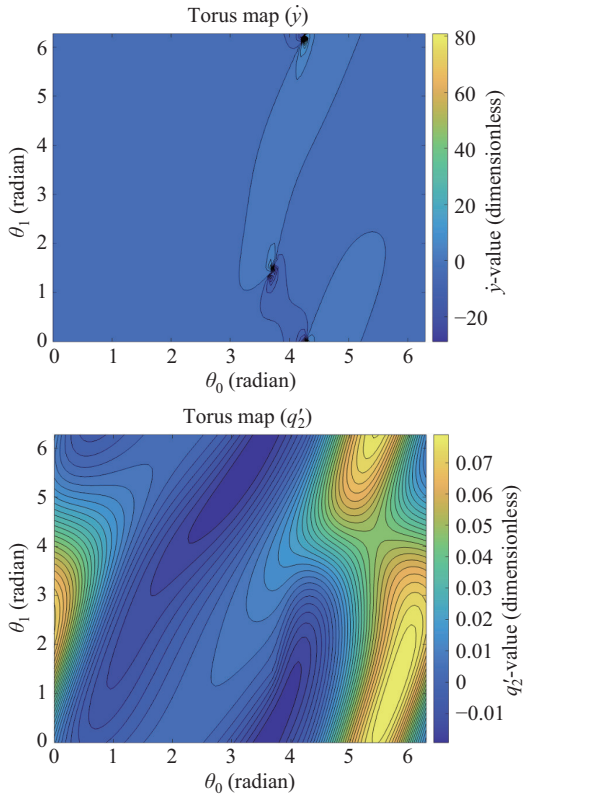

Fig. 6 Torus maps of $\dot{y}$ states at the surface of section before and after regularisation.

If a trajectory belongs to both the stable manifold of one object and the unstable manifold of another, that trajectory would leave one invariant object and then arrive at another in a ballistic fashion, albeit over an infinite time. This type of trajectory is classified as a heteroclinic connection. To find these connections, we must find where stable and unstable manifolds of two objects intersect. This is a non-trivial task for high-dimensional manifolds such as those of quasi-periodic orbits in the CR3BP.

In the CR3BP, spacecraft states are represented by six variables given by the Cartesian position and velocity coordinates as seen from the synodic frame of two attracting masses, such as the Earth and the Moon. The Jacobi integral allows mission designers to express one of the variables as a function of the remaining five. As heteroclinic connections must exist along the hyperbolic manifolds of one or more quasi-periodic orbits, we can reduce the problem to four dimensions by fixing the Jacobi integral and taking a surface of section through which both the stable and unstable manifolds of the objects shall pass. In this work, this surface of section is

placed at $x = 1 - \mu$ (the position of the secondary body on the x-axis). An intersection of the stable and unstable manifolds at this surface of section would constitute a heteroclinic connection. However, data sets of dimension 4 are still difficult to represent in a way that is intuitive to humans.

To determine a heteroclinic connection, we will consider the states of the manifold trajectories at the surface of section, where the propagation ends. We can map the values of y, z, $\dot{x}$, $\dot{y}$, and $\dot{z}$ at the surface of section to the surface of the torus by considering the value of $\boldsymbol{\theta}$ at which each manifold trajectory was initialised, providing a torus map for each variable. The height of the map describes the chosen state variable at the surface of section, while the axes describe where on the torus surface the trajectory departed from. Provided a large number of initialised manifold trajectories, the torus map allows us to interpolate the values of y, z, $\dot{x}$, $\dot{y}$, and $\dot{z}$ at the surface of section for manifold trajectories initialised from anywhere on the torus surface. The function that maps these state variables to the surface of the torus is continuous. Therefore, by selecting one variable to be equal to some arbitrary value we can produce a level curve on the map constructed of all values of $\boldsymbol{\theta}$ which describe a position on the torus surface which would provide that specific value at the surface of section if a manifold trajectory was initialised there. Figure 7 demonstrates this by finding the level curves defined by $z = -0.005$ at the surface of section and using those to interpolate where on the perturbed tori manifold trajectories must be propagated to arrive at the surface of section with a z-value of -0.005 . The variable selected to be used to find the level curves in this way (in this case z) is named the scanning variable, D.

Consider the two sets of D variable values at the surface of section, D_s and D_u, associated with slices of W_s and W_u respectively, and then consider the set $D_\mathrm{s} \cap D_\mathrm{u}$. This set contains every value of D which a heteroclinic connection could have as it passes the surface of section. We then use this range of values to produce level curves on the D variable torus maps. The values of θ_0 and θ_1 that correspond to these curves can be used to interpolate the values of three of the remaining state variables, referred to as A, B, and C, for the same positions on their equivalent torus maps. Due to the nature of continuous functions mapped to compact, boundless manifolds, plotting the interpolated values of A, B, and C provides one or more

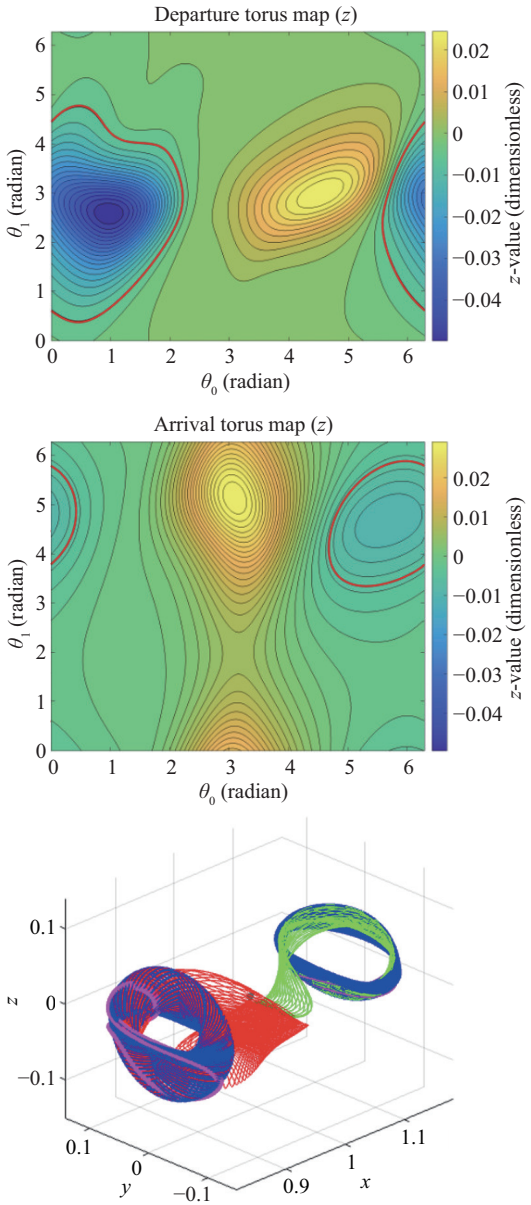

Fig. 7 Level curves of $z = -0.005$ at the surface of section used to interpolate states on the tori's manifolds.

closed curves in a 3-dimensional phase space. Performing this process for both the stable and unstable manifolds produces two sets of these closed curves, named the *stable curves* and *unstable curves*, for which a linking number can be calculated. Figure 8 demonstrates this for A, B, C, and scanning variable D defined by y, $\dot{y}$, $\dot{z}$, and z respectively, thus producing curves in a y–$\dot{y}$–$\dot{z}$ phase space. These curves were constructed using the level curves found in Fig. 7. The linking number of these curves is 1.

Note that for any given set of stable and unstable curves

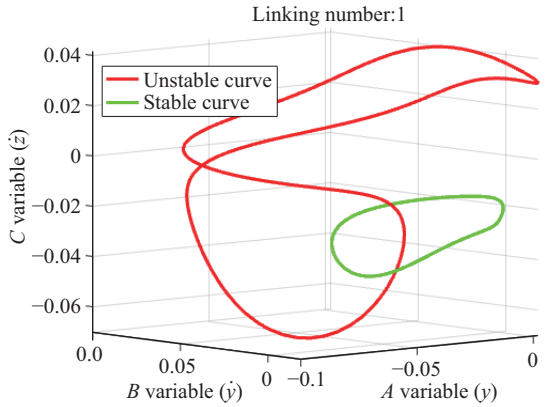

Fig. 8 Example of y–$\dot{y}$–$\dot{z}$ stable and unstable curves interpolated from the $z = -0.005$ level curves in Fig. 7.

we have accounted for x via the surface of section, and the scanning variable D because the curves are interpolated using a unique D value. That means an intersection in stable and unstable curves would constitute a heteroclinic connection, as five state variables would be found to be equal, and the sixth could be calculated using the Jacobi integral of the isoenergetic tori. The challenge then becomes to find intersections of 1-dimensional curves in 3-dimensional space, which is itself challenging as such an intersection would be dimension 0 and require infinite precision to find numerically. However, as discussed previously, the linking number of two closed curves (in this case the stable and unstable curves) can only change if the curves intersect. Therefore, by tracking the linking number of the curves as we vary our D variable, we can easily find with high precision at what value of D the intersection occurs. This method is described in more detail in Section 3.

It is worth noting that while the linking number is typically strictly associated with only *two* closed curves, we are using it here to describe how linked two *sets* of closed curves are; while technically an inaccurate definition of the linking number, this is irrelevant for our purposes as the process still successfully informs us of any intersections that occur between the stable and unstable curves; any change in the linking number of the set is *still* indicative of a heteroclinic connection. We find the linking number of the sets by summing the linking numbers of every combination of stable and unstable curves. For the function $\boldsymbol{K}(\boldsymbol{a}, \boldsymbol{b})$ which outputs the linking number of the curves $\boldsymbol{a}$ and $\boldsymbol{b}$, the linking number equivalent invariant we will instead consider, L, is therefore

$$L = \boldsymbol{K}(\boldsymbol{a}_1, \boldsymbol{b}_1) + \boldsymbol{K}(\boldsymbol{a}_1, \boldsymbol{b}_2) + \cdots + \boldsymbol{K}(\boldsymbol{a}_n, \boldsymbol{b}_{(m-1)}) + \boldsymbol{K}(\boldsymbol{a}_n, \boldsymbol{b}_m) \tag{19}$$

where n and m are the number of curves in sets $\boldsymbol{a}$ and $\boldsymbol{b}$ respectively. It is worth noting that depending on the shape of the manifolds at the crossing of the surface of section, the values of n and m may vary and are not necessarily equal.

3 Methodology

3.1 Calculating the linking number

To calculate the linking number of two closed curves, each closed curve is discretised into line segments. Due to the nature of numerical modelling, the curves are not truly continuous, instead constructed of n points; when using this method to find heteroclinic connections between quasi-periodic orbits, the value of n is determined by the precision of the torus maps, which depends on the density of trajectories used to generate the hyperbolic manifolds of the quasi-periodic orbits; a greater density of trajectories allows us to interpolate more precise level curves on the torus map, and therefore curves with larger values of n.

One of the curves is arbitrarily selected to be converted into a surface constructed of triangles, with the original curve as the boundary of the surface. We choose the stable curve for this. This curve is defined by n line segments constructed of start and end points $[\boldsymbol{p}_j, \boldsymbol{p}_{j+1}]$ for $j = [1, 2, \cdots, n-1]$ and the additional line defined by start and end points $[\boldsymbol{p}_\mathrm{n}, \boldsymbol{p}_1]$, while the unstable curve is defined by m line segments constructed of start and end points $[\boldsymbol{q}_k, \boldsymbol{q}_{k+1}]$ for $k = [1, 2, \cdots, m-1]$ and the additional line defined by start and end points $[\boldsymbol{q}_m, \boldsymbol{q}_1]$. We calculate the mid-point of the curve, $\boldsymbol{P}$, given by

$$\boldsymbol{P} = \sum_{a=1}^{n} \frac{\boldsymbol{p}_a}{n} \tag{20}$$

before constructing n triangles with the line segments of the curve as the bases and $\boldsymbol{P}$ as one of the vertices. The vertices of the triangles would therefore be $[\boldsymbol{p}_j, \boldsymbol{p}_{j+1}, \boldsymbol{P}]$. Each triangle has an associated normal vector $\boldsymbol{R}$, defined as $\boldsymbol{R} = [\boldsymbol{p}_{j+1} - \boldsymbol{p}_j] \times [\boldsymbol{P} - \boldsymbol{p}_{j+1}]$.

For each line segment of the unstable curve we check whether they intersect within any of the triangles that make up the surface of triangles bounded by the stable curve. For a given line segment $\boldsymbol{q}_{k+1} - \boldsymbol{q}_k$, this is achieved by considering the plane the triangle resides in and the

point $\boldsymbol{Q}$ where a vector defined by the line segment would intersect this plane, assuming it is scaled to any length. If the resulting distance between $\boldsymbol{q}_k$ and $\boldsymbol{Q}$ exceeds the length of the line segment, or the distance is negative in the direction of $\boldsymbol{q}_{k+1} - \boldsymbol{q}_k$, the line segment does not intersect the plane. Otherwise, we take three dot products; in each case one vector is a side of the triangle and the other is the vector defined by the first vertices of the side being considered and the point $\boldsymbol{Q}$: $[\boldsymbol{p}_{j+1} - \boldsymbol{p}_j] \cdot [\boldsymbol{Q} - \boldsymbol{p}_j]$, $[\boldsymbol{P} - \boldsymbol{p}_{j+1}] \cdot [\boldsymbol{Q} - \boldsymbol{p}_{j+1}]$, and $[\boldsymbol{p}_{j+1} - \boldsymbol{P}] \cdot [\boldsymbol{Q} - \boldsymbol{P}]$. If all three resulting dot products are positive, the line segment must intersect the interior of the triangle [1].

If an intersection between a line segment and a triangle interior occurs, we use the dot product of the line segment and $\boldsymbol{R}$ to determine the direction through which the line is passing the triangle, where the positive direction is defined as the direction of $\boldsymbol{R}$. Figure 9 shows an example of a positive passing, with an exaggerated scale. Each time an intersection is found, the direction is stored. Once all line segments have been checked against each triangle, positive intersections are given a value of 1, and negative intersections -1. The sum total of all intersections is taken to be the linking number. This process is repeated for each combination of stable and unstable curves, and the combined linking number is taken to the be the linking number of the sets, L.

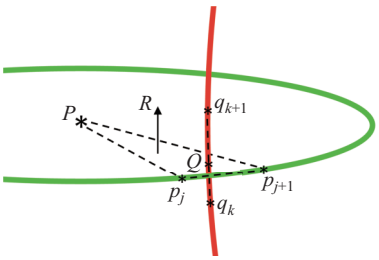

Fig. 9 A positive passing of the unstable curve through the constructed stable curve surface.

This method of calculating the linking number has proven robust during our use, despite what form the linking curves take. While large distortions in the closed curves may result in triangles which appear distant from the smallest surface closed by the curve, ultimately the surface constructed from the triangles will be homeomorphic to a disc and thus the topological qualities that allow the method to work persist.

3.2 Tracking the linking number

In Section 2.4 it is mentioned that D variable level curves, and therefore the stable and unstable curves in the A–B–C phase space, are taken for all D values in $D_s \cap D_u$. In doing so, for each value of D, we now have the tools to calculate the linking number of the associated A–B–C stable and unstable curves. By repeating this process over a dense range of D values, we can track how the curves evolve and see how their linking number changes as the scanning variable varies (Figs. 10 and 11). Provided a dense enough search, we can infer at what values of D changes in the linking number occur to a high precision. Since a change in the linking number is indicative of an intersection in the curves, we can robustly and systematically identify at what values of the scanning variable heteroclinic connections pass the surface of section. Any time a change in the linking number occurs, an average of the D values before and after the change is calculated and taken to be an initial guess for the D value of the heteroclinic connection.

Once these values of D are found, the stable and unstable curves are interpolated for this value and a simple nearest neighbour search is performed to find the points in the curves which are most close to the other set. The average of these points is then taken, providing the A, B, and C values. The Jacobi integral is then used to calculate the remaining coordinate, meaning all six state variables are accounted for and an initial guess for a state along the heteroclinic connection is found.

3.3 Interpolating θ values

We now have an initial guess for the spacecraft state at the surface of section along the heteroclinic connection. However, propagating this state forward and backward in time it is clear that despite passing through the vicinity of the tori, the resulting trajectories do not land on the tori which were used in their generation (Fig. 12), exemplifying the need for differential correction. Even if the result is very close to a state along a connection, confirming whether they arrive at the tori is a complicated task; trajectories do not technically arrive at the torus, only a trajectory on the version of the torus which has been perturbed onto the stable manifold, and this perturbation is selected arbitrarily. Therefore, differential correction would be simpler if we were approaching from another direction: initialising the trajectories on the tori and minimising the difference in the states at the surface of section. An additional step is therefore required to convert our state at the surface of section to two sets of

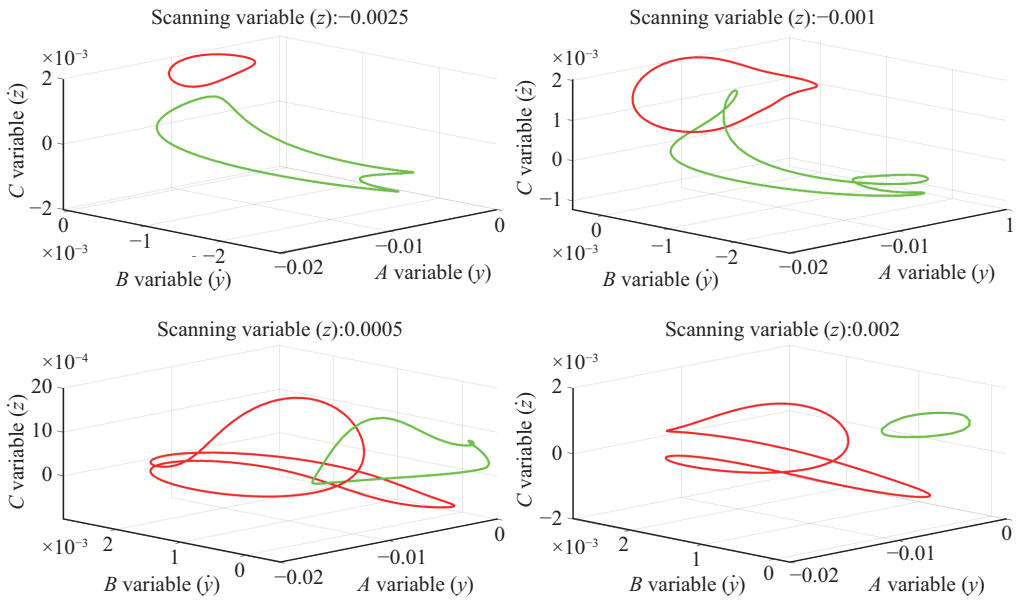

Fig. 10 Evolution of stable and unstable curves as z varies.

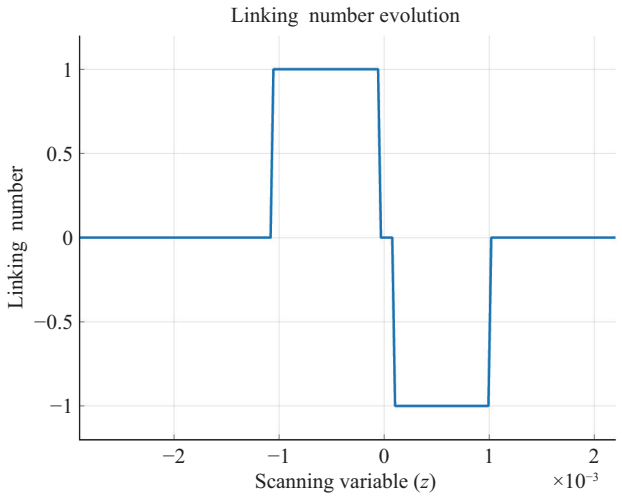

Fig. 11 Evolution of the linking number as z varies, indicating 4 heteroclinic connections.

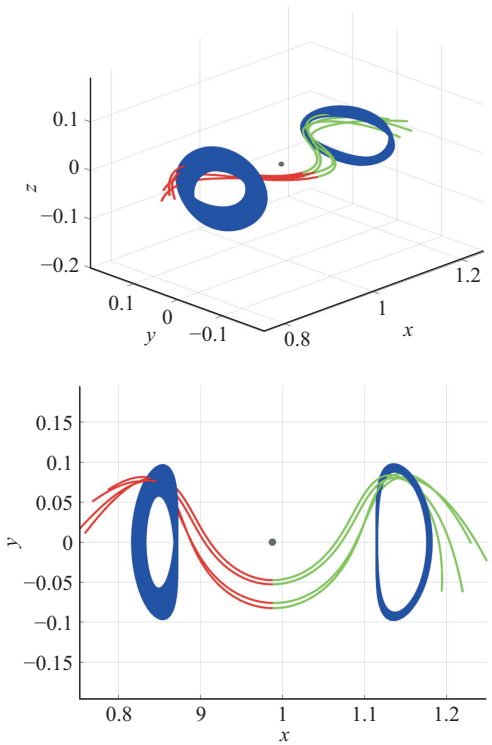

Fig. 12 Four initial guess heteroclinic connections propagated from the surface of section (see Fig. 14 for corrected trajectories).

torus angles which will describe the points of initialisation on the tori from which trajectories are propagated. In short, given some initial guess state at the surface of section $\boldsymbol{X}_i$ we must derive $\boldsymbol{\theta}_\mathrm{s}$ and $\boldsymbol{\theta}_\mathrm{u}$, the torus angles at which our trajectories along the stable and unstable manifolds are initialised respectively. It is likely that no manifold trajectory arrives at the surface of section with an exact state value of $\boldsymbol{X}_i$ as some interpolation is used in generating it, so we must calculate the values of $\boldsymbol{\theta}_\mathrm{s}$ and $\boldsymbol{\theta}_\mathrm{u}$ which produce trajectories that arrive at the surface of section most closely to $\boldsymbol{X}_i$.

This is achieved by plotting level curves on the torus maps of the four state variables used in generating our initial guess at the surface of section $\boldsymbol{X}_i$, A, B, C, and the scanning variable D, and seeing where they overlap for each torus. The level curves extracted from their

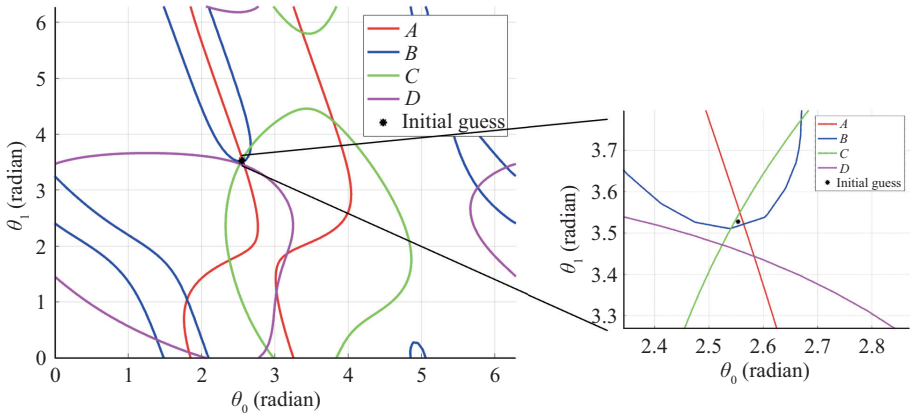

Fig. 13 An initial guess for $\boldsymbol{\theta}$ determined by the intersections of A, B, C, and D level curves on the torus maps of the departing torus.

respective torus maps are defined by their values in $\boldsymbol{X}_i$. For a true map from states on a heteroclinic connection to torus angles we would expect to find all the level curves intersect at a single point. As $\boldsymbol{X}_i$ is not a true state on the torus manifold, we instead find the level curves tend to pass closely to each other in some region but do not intersect at a single point. The goal then is to interpolate a point on the map we deem the centre of this near-passing region.

Given that the curves come together in a single small region, intersections are likely to occur. We will define four classes of intersection: AB intersections are intersections between the A and B level curves, BC intersections are between the B and C level curves, AC intersections are between the and A and C level curves, and D intersections are between D and *any* of the other three curves. Using AB, BC, and AC, we construct every possible triangle that has one vertex from each of these three sets of intersections. We then compare each triangle with each intersection point in D, calculating the distance from each triangle vertex to the D intersection. These three distances are summed. The triangle with the smallest minimum summed distance is taken to be the best candidate for interpolating the torus angles for the initial guess; the mean of the positions of the triangle's vertices is calculated, providing a value of $\boldsymbol{\theta}$. This process is completed for both the departure and arrival tori, yielding $\boldsymbol{\theta}_\mathrm{s}$ and $\boldsymbol{\theta}_\mathrm{u}$.

This method of interpolating the $\boldsymbol{\theta}$ values of the initial guess is limited. The level curves generated using the variables of $\boldsymbol{X}_i$ do not necessarily have to intersect or intersections hypothetically could occur far from the true location of the heteroclinic connection on the torus map depending on the intersection angle of the curves. While these issues have not become apparent throughout our investigation, for these reasons a more robust method of interpolating these values is in development.

3.4 Differential correction

Given that we have generated initial guesses for $\boldsymbol{\theta}_\mathrm{s}$ and $\boldsymbol{\theta}_\mathrm{u}$, we can differentially correct these values to produce a heteroclinic connection. This is achieved by initialising trajectories on the stable and unstable manifolds of the respective tori and propagating them to the surface of section, then minimising the difference in the trajectory states at that surface. Unlike Henry and Scheeres [17], who included the propagation time to the surface of section, we are choosing to end the propagation at the surface of section, removing the need for these two additional variables in the correction process.

We define a function Ψ that maps the torus angles at which a manifold trajectory is initialised to the trajectory's state at the surface of section.

$$\Psi(\boldsymbol{\theta}) = \Psi(\theta_0, \theta_1) = \boldsymbol{X} \tag{21}$$

The initialised manifold trajectory is found via interpolation of the torus maps. While this can lead to issues with preservation of the Jacobi integral if the scaling factor of the perturbation onto the manifold is large, we have found a perturbation of magnitude 10^{-6} is small enough to avoid any large discrepancies in Jacobi integrals which may prevent the correction of heteroclinic connections.

For a heteroclinic connection to be found, the following equation must be satisfied:

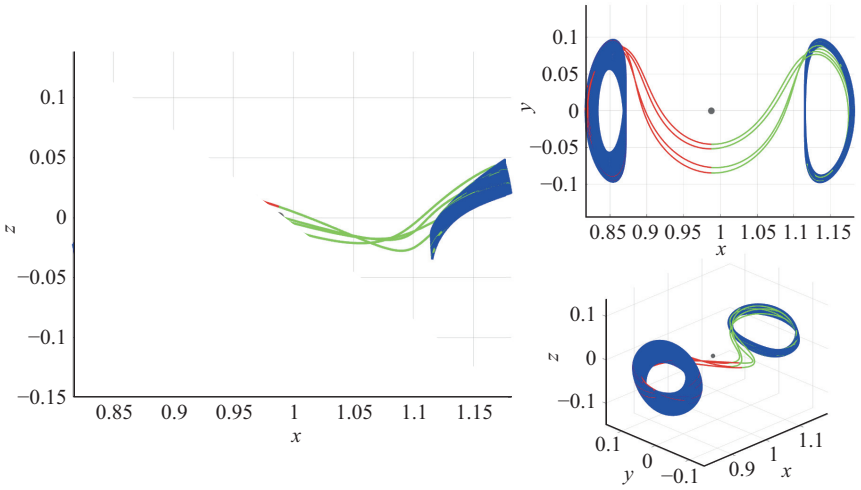

Fig. 14 Heteroclinic connections between quasi-halo orbits in the Earth–Moon system.

$$\Psi_{\mathrm{s}}(\boldsymbol{\theta}_{\mathrm{s}}) - \Psi_{\mathrm{u}}(\boldsymbol{\theta}_{\mathrm{u}}) = \boldsymbol{X}_{\mathrm{s}} - \boldsymbol{X}_{\mathrm{u}} = 0 \tag{22}$$

This constraint allows us to construct a boundary value problem which can be easily solved using freely available nonlinear equation solvers from existing MATLAB libraries, such as "fsolve".

4 Applications

4.1 Earth–Moon

In this section we consider connections between quasi-halo and Lissajous orbits within the vicinity of the Moon in the Earth–Moon system. The mass ratio parameter μ was defined as 0.012153643. All example connections in the Earth–Moon system presented in this paper have a Jacobi integral of 3.15.

4.1.1 Quasi-halo to quasi-halo

Quasi-halo to quasi-halo trajectories are the simplest form of heteroclinic connections found in the Earth–Moon system as they do not require multiple crossings of the surface of section.

Four connections can be found for L1 orbit and L2 orbit latitudinal frequencies of 0.2739 and 0.02163 respectively, seen in Fig. 14, matching the number of linking number changes in Fig. 15.

4.1.2 Lissajous to Lissajous

It is often the case that heteroclinic connections between Lissajous orbits in the Earth–Moon system do not exist for trajectories that pass the surface of section $x = 1 - \mu$ only once [5] depending on the energy and frequency of the orbits. Therefore, to demonstrate the

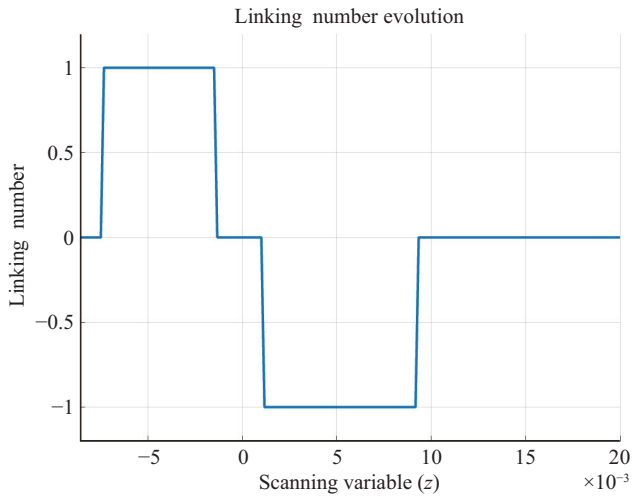

Fig. 15 Evolution of the linking number associated with the orbits in Fig. 14.

method's robustness, torus maps are constructed using state variables at the second passing of the surface of section when interpolating the linking curves in this example.

Eight connections can be found for L1 orbit and L2 orbit latitudinal frequencies of 0.3226 and 0.3578 respectively, seen in Fig. 16, matching the number of linking number changes in Fig. 17. Lissajous orbits have symmetric properties through the x–y plane. As such, we find that each heteroclinic connection between two Lissajous orbits is part of a pair of trajectories, reflected through the x–y plane (Fig. 16). This is also clear in the evolution of the linking number when z is chosen as the scanning variable D (Fig. 17), as we see changes in the linking number occur twice at values of z with

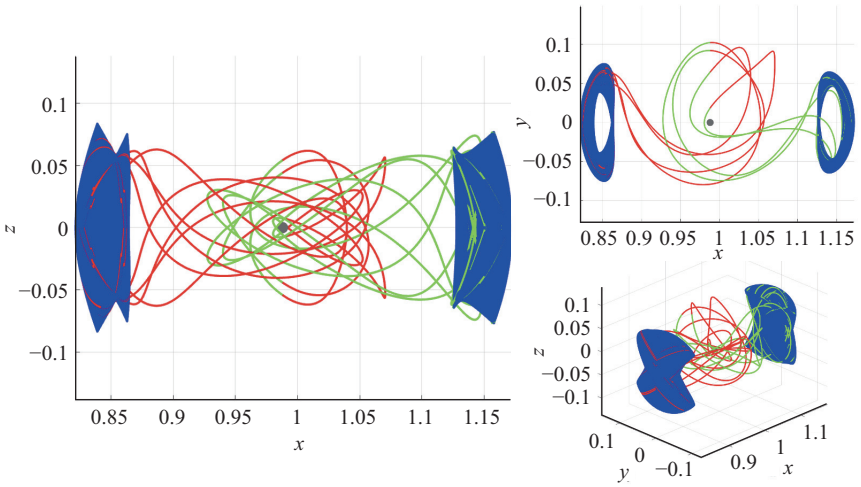

Fig. 16 Heteroclinic connections between Lissajous orbits in the Earth–Moon system.

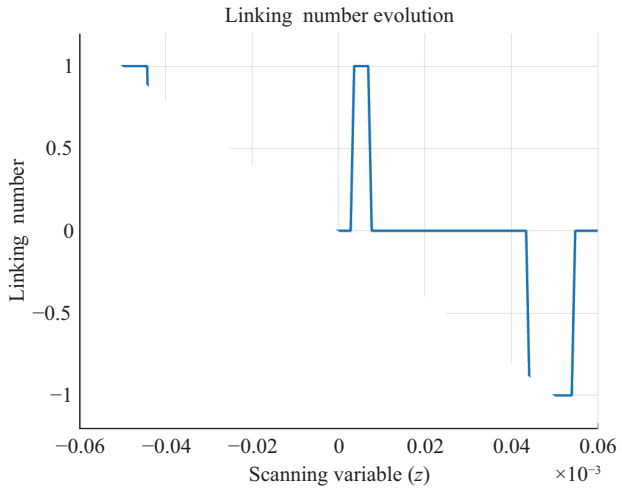

Fig. 17 Evolution of the linking number associated with the orbits in Fig. 16.

equal magnitude but opposite sign. This raises concerns regarding the choice of scanning variable D; if any value besides z or $\dot{z}$ was chosen as the scanning variable, the linking curves would experience two intersections at the same value of D, and the process would likely fail to detect both. This can be mitigated by assuring z or $\dot{z}$ are selected as the scanning variable when trying to find connections between two orbits with symmetry through the x–y plane, such as Lissajous orbits.

4.1.3 Quasi-halo to Lissajous

Like in the case of Lissajous to Lissajous heteroclinic connections in the Earth–Moon system, quasi-halo to Lissajous connections often require an additional passing of the surface of section. However, while the invariant manifolds of Lissajous orbits typically return fully to the surface of section without leaving the vicinity of the Moon, the manifolds of quasi-halo orbits in the Earth–Moon system often separate after the initial passing into groups of trajectories which either quickly intersect the surface of section a second time or depart from the Moon before intersecting the surface much later. While the manifold itself always remains continuous even in this case, a 2-dimensional section of such a manifold is not continuous. This means we cannot properly interpolate level curves using torus maps of these orbits. This problem is discussed further in Section 5.

4.2 Sun–Earth

In this section we briefly consider two Lissajous orbits within the vicinity of the Earth in the Sun–Earth system. Transfers to, from, and between libration point orbits in the Sun–Earth system have been demonstrated by past missions [19]. The mass ratio parameter μ was defined as 3.039548×10^{-6}. All example connections in the Sun–Earth system presented in this paper have a Jacobi integral of 3.00065.

4.2.1 Lissajous to Lissajous

Eight connections can be found for L1 orbit and L2 orbit latitudinal frequencies of 0.4573 and 0.4608 respectively, seen in Fig. 18. Figure 19 seems to show only 6 discrete changes in the linking number, though two of the changes appear to be directly from -1 to 1. An increase in the density of D-values reveals discrete changes between -1 and 0, and 0 and 1, in very close succession. This is

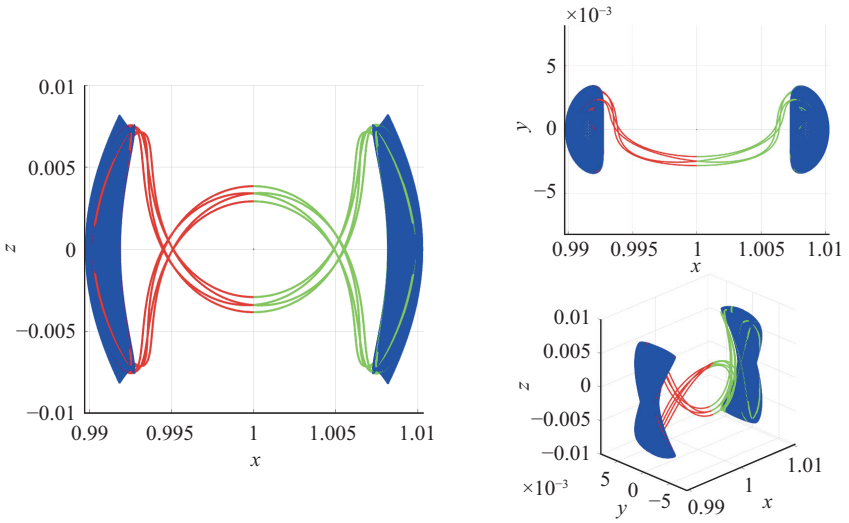

Fig. 18 Heteroclinic connections between Lissajous orbits in the Sun–Earth system.

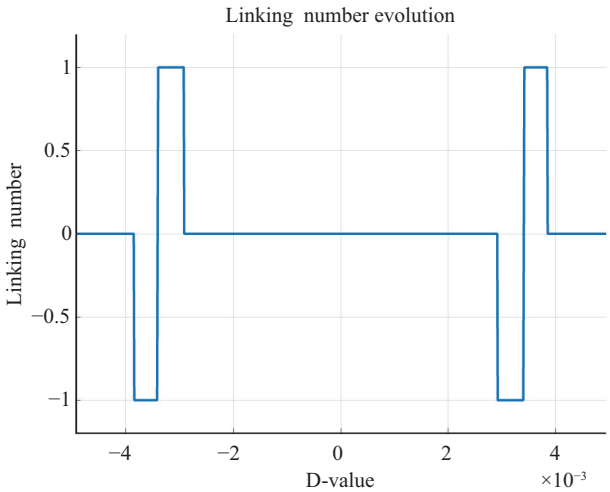

Fig. 19 Evolution of the linking number associated with the orbits in Fig. 18.

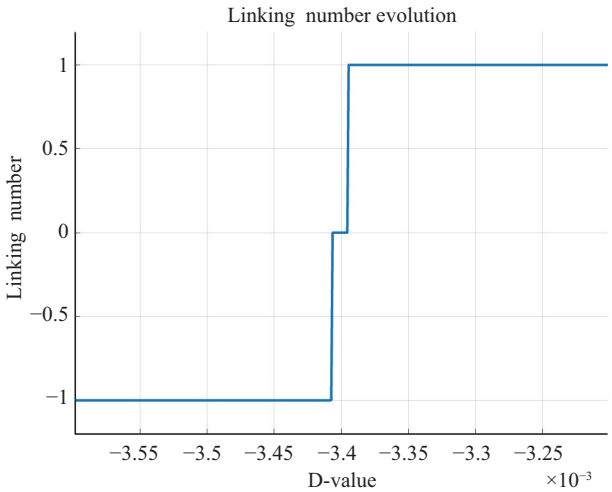

Fig. 20 Enlarged image of Fig. 19.

shown in Fig. 20, which is an enlarged image of the first magnitude 2 change in Fig. 19.

A notable difference between these heteroclinic connections and those of Lissajous orbits in the Earth–Moon system is that the transfers do not require an additional passing of the surface of section. As is the case for the Earth–Moon system, Lissajous to Lissajous connections in the Sun–Earth system belong to pairs of symmetric trajectories mirrored through the x–y plane.

4.2.2 Quasi-halo to Lissajous

Unlike in the Earth–Moon system, quasi-halo to Lissajous transfers in the Sun–Earth system do not require multiple crossings of the surface of section for the selected energy level and frequency. The issues encountered regarding discontinuities in the torus maps are alleviated and transfers can be easily found.

Four connections can be found for for L1 orbit and L2 orbit latitudinal frequencies of 0.3745 and 0.4224 respectively, seen in Fig. 21, matching the number of linking number changes in Fig. 22.

4.3 Jupiter–Ganymede

In this section we briefly consider two quasi-halo orbits within the vicinity of the Galilean moon Ganymede in the Jupiter–Ganymede system. The mass ratio parameter μ was defined as 7.807083×10^{-5}. All example connections in the Jupiter–Ganymede system presented in this paper have a Jacobi integral of 3.0066.

Four connections can be found for for L1 orbit and

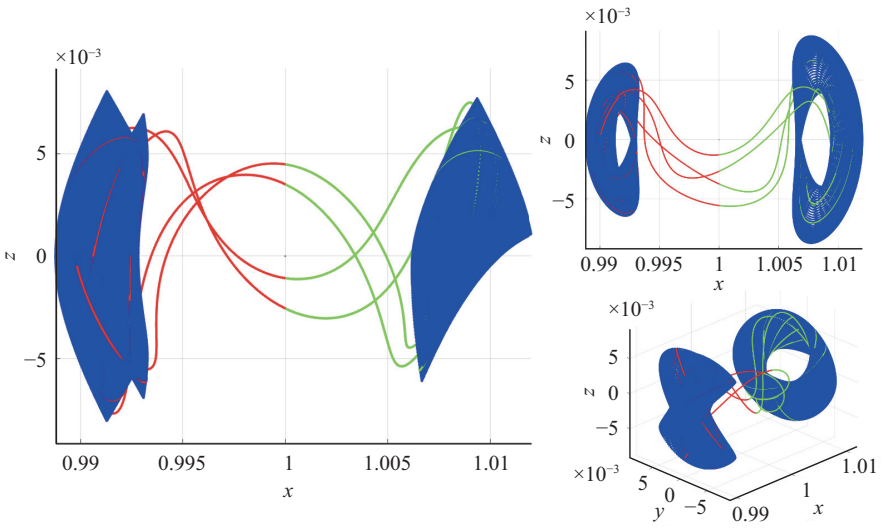

Fig. 21 Heteroclinic connections between a quasi-halo orbit and a Lissajous orbit in the Sun–Earth system.

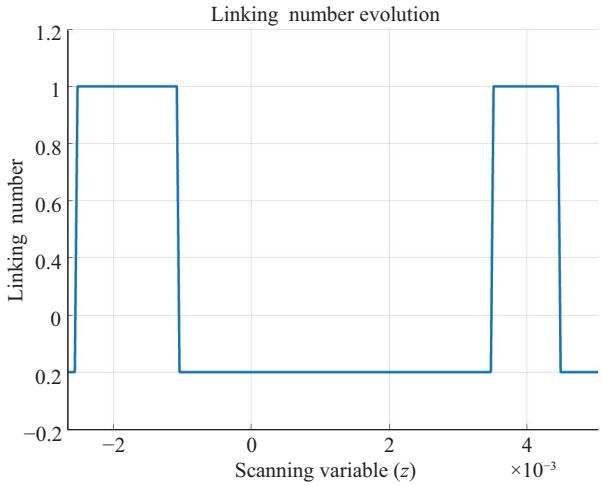

Fig. 22 Evolution of the linking number associated with the orbits in Fig. 21.

L2 orbit latitudinal frequencies of 0.1787 and 0.0957 respectively, matching the number of linking number changes in Fig. 24. The shape of the connections and the number of them reflect closely those of the quasi-halo orbits in the Earth–Moon system.

5 Discussion

Section 4 demonstrates the effectiveness of the linking number method for detecting heteroclinic connections in the CR3BP for various mass ratio parameters, energy levels, and tori frequencies. By informed selection of an appropriate scanning variable and surface of section, the knot theory approach plainly provides the exact number of connections available between a pair of isoenergetic quasi-periodic orbits in the form of the evolution of the linking number (Figs. 15, 17, 19, 24), from which initial guesses can be extracted for differential correction. The accuracy of these initial guesses is quantified by the magnitude of the difference between the state vectors of the initial guess trajectories from the stable and unstable manifolds at the surface of section; this difference typically has an order of magnitude between 10^{-6} and 10^{-4} in non-dimensional units.

One limitation of this method is the reliance on the continuity of the torus maps to ensure the linking curves are themselves both continuous and closed, which are required for accurate calculation of the linking numbers. The invariant manifolds of some orbits, particularly quasi-halo orbits in the Earth–Moon system, tend to separate after the initial passing of the surface of section $x = 1-\mu$; some trajectories return quickly to the surface of section, while others first depart from the vicinity of the Moon before eventually passing the surface again much later (Fig. 25).

This results in torus maps which describe the state of the manifold at the second surface passing to become discontinuous, at which point the interpolated linking curves are no longer continuous closed manifolds and the concept of a linking number cannot be usefully applied. This shortcoming is only relevant when attempting to detect heteroclinic connections which pass the surface of section multiple times, such as in the case of quasi-halo to Lissajous transfers in the Earth–Moon system.

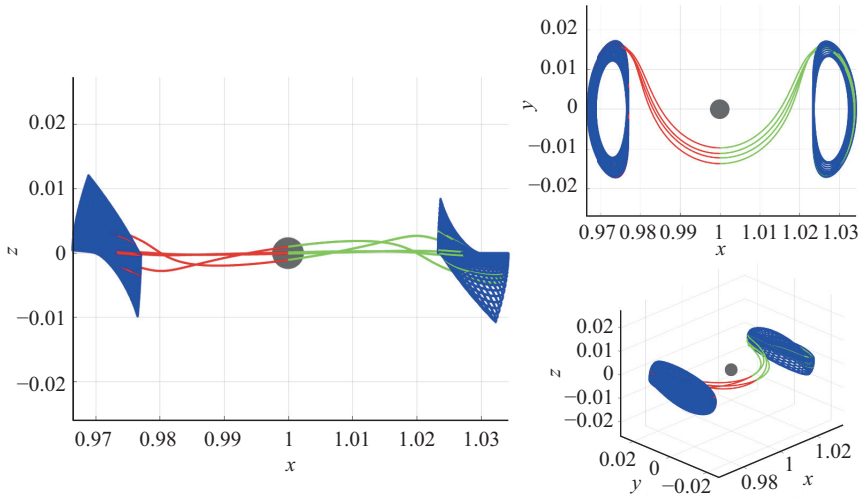

Fig. 23 Heteroclinic connections between quasi-halo orbits in the Jupiter–Ganymede system.

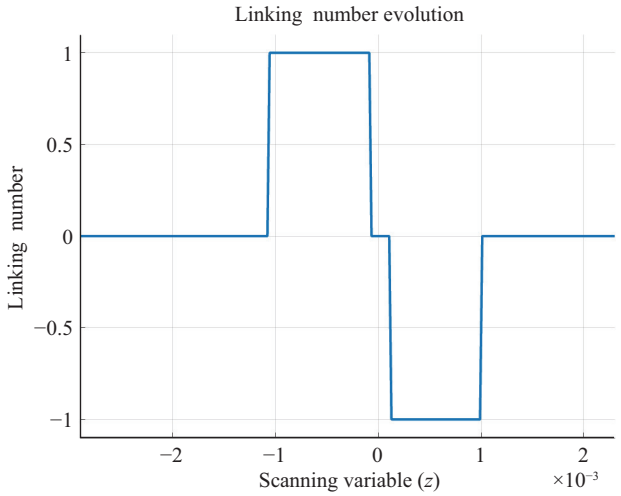

Fig. 24 Evolution of the linking number associated with the orbits in Fig. 23.

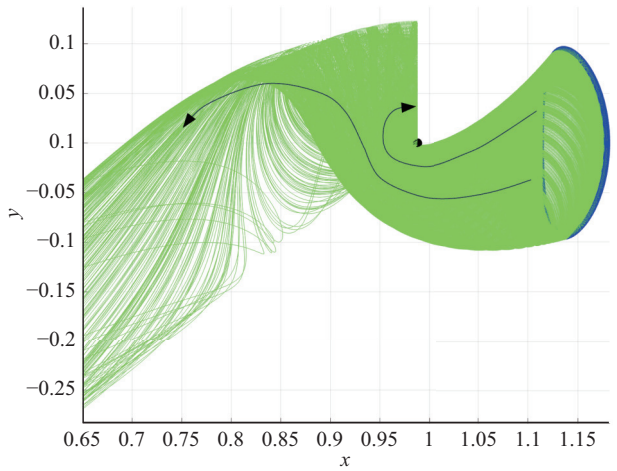

Fig. 25 Separation of quasi-periodic halo orbit manifold after first passing of $x = 1 - \mu$.

This issue may be avoided by future consideration of other surfaces of section, such as periapsis or apoapsis maps. However, these have their own issues in use with the approach presented in this work; in the case of periapsis/apoapsis maps, manifold trajectories may encounter a periapsis/apoapsis during its initial time spent in the vicinity of the libration orbit before properly departing depending on the size of the perturbation onto the invariant manifold surface, resulting in sets of periapses/apoapses which are non-continuous.

6 Conclusions

This work describes a method of robustly detecting heteroclinic connections between isoenergetic quasi-periodic tori in the circular restricted three-body problem (CR3BP). Using previously established methods of propagating the hyperbolic manifolds of said orbits to a surface of section, states at this surface are then mapped to the tori surfaces. From these surfaces, curves associated with both the stable and unstable manifolds are interpolated, for which we know an intersection of the curves would constitute a heteroclinic transfer. By tracking the topological property known as the linking number as these curves evolve, we show that it is possible to precisely predict at what states the manifolds intersect at the surface of section, from which highly accurate initial guesses for the heteroclinic connections are deduced and differentially corrected. This knot theory approach was shown to be effective for detecting heteroclinic connections in the CR3BP for various mass

ratio parameters, energy levels, and tori frequencies, in the case of the Earth–Moon, Sun–Earth, and Jupiter–Ganymede systems.

In this paper, we used 1-dimensional closed curves in a 3-dimensional phase space to calculate the linking number for applications in the CR3BP. However, curves and phase space of these dimensions would not be applicable to find heteroclinic connections in non-autonomous Hamiltonian systems such as the bicircular restricted four-body problem due to the additional dimension of time and the lack of an integral of motion. However, the linking number has equivalents in higher dimensions which may allow a similar method to be applied to aid in the detection of heteroclinic connections in higher-fidelity models. Expansion of this method to non-autonomous Hamiltonian systems will be the focus of future work, along with mitigation strategies for the shortcomings highlighted in the case of torus maps for multiple surface of section crossings.

Declaration of competing interest

The authors have no competing interests to declare that are relevant to the content of this article.

References

[1] Amanatides, J., Choi, K. Ray tracing triangular meshes. In: Proceedings of the 8th Western Computer Graphics Symposium, **1997**.

[2] Anderson, R. L. Tour design using resonant-orbit invariant manifolds in patched circular restricted three-body problems. *Journal of Guidance, Control, and Dynamics*, **2021**, 44(1): 106–119.

[3] Anderson, R. L., Lo, M. W. Flyby design using heteroclinic and homoclinic connections of unstable resonant orbits. In: Proceedings of the 21st AAS/AIAA Space Flight Mechanics Meeting, **2011**: AAS11-125.

[4] Angelopoulos, V. The ARTEMIS mission. In: *The ARTEMIS Mission*. Russell, C., Angelopoulos, V., Eds. New York: Springer, **2010**: 3–25.

[5] Arona, L., Masdemont, J. J. Computation of heteroclinic orbits between normally hyperbolic invariant 3-spheres foliated by 2-dimensional invariant Tori in Hill's problem. In: *Conference Publications*. American Institute of Mathematical Sciences, **2007**: 64–74.

[6] Barcelona, M., Haro, A., Mondelo, J. M. Semianalytical computation of heteroclinic connections between center manifolds with the parameterization method. *SIAM Journal on Applied Dynamical Systems*, **2024**, 23(1): 98–126.

[7] Bonasera, S., Bosanac, N. Transitions between quasi-periodic orbits near resonances in the circular restricted three-body problem. In: Proceedings of the AAS/AIAA Astrodynamics Specialist Virtual Conference, **2020**: AAS 20-724.

[8] Broschart, S. B., Chung, M. K. J., Hatch, S. J., Ma, J. H., Sweetser, T. H., Weinstein-Weiss, S. S., Angelopoulos, V. Preliminary trajectory design for the Artemis lunar mission. *Advances in the Astronautical Sciences*, **2009**, 135(2): 1329–1343.

[9] Calleja, R. C., Doedel, E. J., Humphries, A. R., Lemus-Rodríguez, A., Oldeman, E. B. Boundary-value problem formulations for computing invariant manifolds and connecting orbits in the circular restricted three body problem. *Celestial Mechanics and Dynamical Astronomy*, **2012**, 114(1): 77–106.

[10] Celletti, A. Basics of regularization theory. In: *Chaotic Worlds: from Order to Disorder in Gravitational N-Body Dynamical Systems*. Steves, B. A., *et al.*, Eds. Dordrecht: Springer Netherlands, **2003**: 203–230.

[11] De Smet, S., Scheeres, D. J. Identifying heteroclinic connections using artificial neural networks. *Acta Astronautica*, **2019**, 161: 192–199.

[12] Delshams, A., Masdemont, J. J., Roldán, P. Computing the scattering map in the spatial Hill's problem. *Discrete and Continuous Dynamical Systems - B*, **2008**, 10(2–3): 455–483.

[13] Gómez, G., Llibre, J., Masdemont, J. Homoclinic and heteroclinic solutions in the restricted three-body problem. *Celestial Mechanics*, **1988**, 44(3): 239–259.

[14] Gómez, G., Masdemont, J. Some zero cost transfers between libration point orbits. *Advances in the Astronautical Sciences*, **2000**, 105(2): 1199–1216.

[15] Haapala, A., Howell, K. C. Trajectory design using periapse Poincaré maps and invariant manifolds. In: Proceedings of the 21st AAS/AIAA Space Flight Mechanics Meeting, **2011**: AAS 11-131.

[16] Haapala, A. F., Howell, K. C. Representations of higher-dimensional Poincaré maps with applications to spacecraft trajectory design. *Acta Astronautica*, **2014**, 96: 23–41.

[17] Henry, D. B., Scheeres, D. J. A survey of heteroclinic connections in the Earth–Moon system. In: Proceedings of the 73rd International Astronautical Congress, **2022**: IAC-22,C1,9,3,x70258.

[18] Henry, D. B., Scheeres, D. J. Quasi-periodic orbit transfer design via whisker intersection sets. *Journal of Guidance, Control, and Dynamics*, **2023**, 46(10): 1929–1944.

[19] Koon, W. S., Lo, M. W., Marsden, J. E., Ross, S. D. The Genesis trajectory and heteroclinic connections. In: Proceedings of the AAS/AIAA Astrodynamics Specialist

Conference, **1999**: 99–451.

[20] Koon, W. S., Lo, M. W., Marsden, J. E., Ross, S. D. Dynamical systems, the three-body problem and space mission design. In: *Equadiff 99*. World Scientific Publishing Company, **2000**: 1167–1181.

[21] Kumar, B., Anderson, R. L., de la Llave, R. High-order resonant orbit manifold expansions for mission design in the planar circular restricted 3-body problem. *Communications in Nonlinear Science and Numerical Simulation*, **2021**, 97: 105691.

[22] Kustaanheimo, P., Schinzel, A., Davenport, H., Stiefel, E. Perturbation theory of Kepler motion based on spinor regularization. *Journal für die reine und angewandte Mathematik*, **1965**, 1965(218): 204–219.

[23] Masdemont, J. J. High-order expansions of invariant manifolds of libration point orbits with applications to mission design. *Dynamical Systems*, **2005**, 20(1): 59–113.

[24] McCarthy, B., Howell, K. Construction of heteroclinic connections between quasi-periodic orbits in the three-body problem. *The Journal of the Astronautical Sciences*, **2023**, 70(4): 24.

[25] Olikara, Z. P. Computation of quasi-periodic tori and heteroclinic connections in astrodynamics using collocation techniques. Ph.D. Thesis. University of Colorado at Boulder, **2016**.

[26] Olikara, Z. P.; Scheeres, D. J. Numerical method for computing quasi-periodic orbits and their stability in the restricted three-body problem. *Advances in the Astronautical Sciences*, **2012**, 145: 911–930.

[27] Ricca, R. L., Nipoti, B. Gauss' linking number revisited. *Journal of Knot Theory and Its Ramifications*, **2011**, 20(10): 1325–1343.

[28] Shonkwiler, C., Vela-Vick, D. S. Higher-dimensional linking integrals. *Proceedings of the American Mathematical Society*, **2011**, 139(4): 1511.

[29] Smith, M., Craig, D., Herrmann, N., Mahoney, E., Krezel, J., McIntyre, N., Goodliff, K. The Artemis program: An overview of NASA's activities to return humans to the Moon. In: Proceedings of the IEEE Aerospace Conference, **2020**: 1–10.

[30] Stiefel, E. L., Scheifele, G. *Linear and Regular Celestial Mechanics: Perturbed Two-Body Motion Numerical Methods Canonical Theory*. Springer Berlin, Heidelberg, **1971**.

Danny Owen is a Ph.D. candidate at the Surrey Space Centre. He received his bachelor degree in physics with planetary science from the University of Leicester and his master degree in space engineering from the University of Surrey. His research interests include application of dynamical system theory to multi-body regimes and multi-parameter continuation methods. E-mail: danny.owen@surrey.ac.uk

Nicola Baresi graduated from the University of Colorado Boulder with a Ph.D. degree in astrodynamics and satellite navigation systems. He was later employed at the Japanese Aerospace Exploration Agency (JAXA), working on small and large scale satellite missions to the Moon and Mars. Since 2019, he has joined the University of Surrey, where he is now a lecturer in orbital mechanics at the Surrey Space Centre. E-mail: n.baresi@surrey.ac.uk